Simulating Ferro- & Antiferromagnetic to paramagnetic phase transitions using a 2D Ising model

Jochem Langen
Physics Department, Durham University, United Kingdom
(Submitted: 26-07-2022)

In this work, computational simulations of the 2D ising model are compared to theory of anti- and ferromagnetic phase transitions to paramagnetism. The critical exponents of the magnetic susceptibility are found to be higher for the paramagnetic phase and lower for the ferromagnetic phase of the ferromagnet. For the antiferromagnet, the critical exponent in the paramagnetic phase has been found to be lower and the quadratic model of the antiferromagnetic phase does not fit the data well.

I Introduction

In a ferromagnet, the magnetic moment of the particles in the lattice of the solid align due exchange interaction energy between them, creating spontaneous magnetisation. In an antiferromagnet this interaction is of opposite sign, causing the moments to anti-align, resisting magnetisation of the material. These materials show a 2nd order phase transition to paramagnetism, where magnetisation does not arise spontaneously but in response to an external magnetic field.
In this work, computational results of the Metropolis algorithm on a 2D Ising solid are investigated and compared to analytical theories of the (anti-)ferro- to paramagnetic phase transitions. In particular, the critical exponent γ of the magnetic susceptibility χ is looked into.

I.1 Ising model

The Ising model predicts the magnetic behaviour of a crystal as a lattice of spin particles, i.e. particles with zero orbital angular momentum, working in the canonical ensemble [1]. Neglecting the diamagnetic response, this gives an Hamiltonian of the system with an Heisenberg exchange and paramagnetic term: [1, 2, 3]

$$\hat{\mathcal{H}} = -J_{eff} \sum_{\langle i,j \rangle}^{N} \vec{\mathbf{S_i}} \cdot \vec{\mathbf{S_j}} - \mu \sum_{i}^{N} \vec{\mathbf{B}} \cdot \vec{\mathbf{S_i}}. \tag{1}$$

This expression is for an isotropic homogeneous system of N particles where we consider the nearest neighbours, $\langle i, j \rangle$, exchange interaction only. Here, $\vec{\mathbf{S_i}}$ is a unit spin vector, J_{eff} the effective exchange energy, μ the magnetic moment of a spin particle and $\vec{\mathbf{B}}$ the magnetic field vector. In this work the 2D Ising model will be investigated, having spins along the z-axis on a 2D lattice in the xy-plane with $\vec{\mathbf{B}}$ either parallel or anti-parallel to the spins. Additionally, periodic boundary conditions are imposed such that spin interaction loops around on both axes, making the lattice form a toroid in 3D [4]. This simplifies the system as each spin particle can be treated the same. Note that the difference in free energy between periodic and free, non-looping, boundary conditions should go to zero in the thermodynamic limit ($N \to \infty$), thus giving the same macroscopic properties of this system [4]. The described system can be seen in fig. 1.
The relative magnetisation of the lattice is determined as follows: [2, 5]

$$\frac{M}{M_s} = \frac{n\bar{\mu}_z}{n\mu} = \bar{S}_z = \bar{s} = \frac{1}{N} \sum_{i}^{N} s_i, \tag{2}$$

where M is the magnetisation, M_s the saturation magnetisation, $\langle \mu_z \rangle$ & $\bar{s} \equiv \bar{S}_z$ the z-component of the

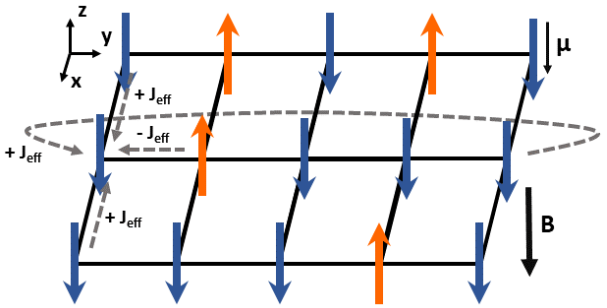

Figure 1: A 2D Ising model 5×3 spin lattice under a magnetic field B with spin magnetic moment μ and homogeneous isotropic exchange interaction energy J_{eff}.

magnetic moment & spin vector averaged over the entire lattice and n the number density of spin particles. The magnetic susceptibility of the system is given through the fluctuation-dissipation theorem, which enables us to determine non-equilibrium properties of the system, subjected to an external magnetic force, from the thermal fluctuations in its equilibrium state [6]. This allows us to define an effective magnetic susceptibility χ_{eff} : [4, 6, 7, 8]

$$\chi_{eff} = \frac{N|J_{eff}|}{k_B T} \left(\left\langle \left(\frac{M}{M_s} \right)^2 \right\rangle - \left\langle \frac{M}{M_s} \right\rangle^2 \right), \tag{3}$$

where k_B is the Boltzmann constant and $\left\langle \frac{M}{M_s} \right\rangle$ is the relative magnetisation averaged over these thermal fluctuations. The definition including $|J_{eff}|$ has been chosen so that the combined variable $\frac{k_B T}{|J_{eff}|}$ can be used.

I.1.1 Analytical solution for the ferromagnet

The analytical solution to the ($B = 0T$) 1D Ising model had been found by Ising himself in 1925, though it did not exhibit a phase transition at finite T [2, 6]. However, the model does show this behaviour for higher dimensions and the analytical solution for the free energy, giving the magnetisation, for the 2D model had been found in 1943, derived by Onsager [6]. This resulted in the following expression for the relative magnetisation in the thermodynamic limit: [4, 9]

$$\frac{M}{M_s} = \pm \frac{(1+z^2)^{0.25}(1-6z^2+z^4)^{0.125}}{\sqrt{1-z^2}}, \tag{4}$$

where $z = e^{-2J/k_B T}$. This equation has a root at $\frac{k_B T_c}{J} \approx 2.269$, giving us the critical (or Curie) temperature T_c of the ferro- to paramagnetic phase transition. The solution predicts this to be a 2nd order phase transition as the magnetisation is a continuous function to T_c.

For the zero-field magnetic susceptibility the following

relations were found: [4, 6]

$$\chi_0 \approx \frac{N\mu^2}{k_B T_c} \times \begin{cases} C_+ \left(\frac{T_c}{T-T_c}\right)^{\frac{7}{4}} for\ T > T_c \\ C_- \left(\frac{T_c}{|T-T_c|}\right)^{\frac{7}{4}} for\ T < T_c \end{cases}, \quad (5)$$

where C_+ & C_- are constants of ≈ 0.96258 & ≈ 0.02554 respectively, giving a ratio of $\frac{C_+}{C_-} \approx 37.689$. The model also predicts the following proportionality for the correlation length, ζ: [6]

$$\zeta \propto \frac{1}{T-T_c}, \quad (6)$$

which describes the length to which spins are correlated.

I.1.2 Other theories

Much earlier, a solution which also works for a 3D solid with an Hamiltonian as described in eq. 1 was found by Curie and Weiss. Their mean field theory assumes only small fluctuations in magnetisation in the system away from the total average magnetisation [2]. This gives rise to the approximation that each atom experiences an internal uniform B-field caused by the magnetisation, called the molecular field [5]. For a ferromagnet, this theory predicts the behaviour of χ_0 above T_c as the Curie-Weiss law. Additionally Landau's theory of 2nd order phase transitions extends this to the region below T_c adding in a factor of $\frac{1}{2}$ to the constant of proportionality C, called the Curie constant [6]. So for the entire range of T we get:

$$\chi_0 = \begin{cases} \frac{C}{T-T_c}\ for\ T > T_c \\ \\ \frac{C/2}{|T-T_c|}\ for\ T < T_c \end{cases}. \quad (7)$$

I.1.3 Analytical solution for antiferromagnetism

The mean-field theory can be extended to antiferromagnetism, where it predicts χ_0 to be: [5]

$$\chi_0 = \frac{C}{T+T_N} \quad (8)$$

for $T \geq T_N$, where T_N is the Néel temperature which should be equal to T_c. For the regime below T_N, Néel's theory predicts χ_0 to be a continuous function from $T = T_N$ to $T = 0\ K$ where $\chi_0 = 0$ for a magnetic field on the same axis as the spins [5]. Additionally, from Heller & Kramer's spin wave method, a more exact relation for $T \leq T_N$ can be obtained for a simple cubic lattice: [10]

$$\chi_0 \propto T^2. \quad (9)$$

II Methods

II.1 Metropolis Algorithm

The computational results of the simulated Ising model as described in section I.1 are obtained using the Metropolis Algorithm. This algorithm is a modified Monte Carlo integration over configuration space of a system [11]. It changes the spin configurations such that on average it follows the Boltzmann distribution, which describes the Ising system [1]. The Metropolis Algorithm works thus: [1, 6]

1. An initial (pseudo-)random spin configuration is created.
2. A thermal sweep is performed, cycling through all spins:
   (a) The sign of the spin is flipped.
   (b) The relative probability $\mathcal{R}$ of the spin flip is calculated.
   (c) If this is bigger than 1, we move onto the next particle.
   (d) If not, a (pseudo-)random number between 0 and 1 is generated.
   (e) If $\mathcal{R}$ is smaller than this random number the sign is flipped back, otherwise we move onto the next particle.

The (pseudo-)random numbers are generated using the NumPy.random library. Here $\mathcal{R}$ is calculated from the thermal probability $p_{\{s_i\}}$ of the configuration state $\{s_i\}$:

$$\mathcal{R} = \frac{p_{\{s_i\},fl}}{p_{\{s_i\}}} = \frac{\frac{exp(-\beta E_{\{s_i\},fl})}{Z}}{\frac{exp(-\beta E_{\{s_i\}})}{Z}} = e^{-\beta(E_{\{s_i\},fl} - E_{\{s_i\}})}, \quad (10)$$

where $E_{\{s_i\},fl}$ is the energy of the configuration with this specific spin flipped and β has the usual thermodynamic definition. This energy difference $\Delta E = E_{\{s_i\},fl} - E_{\{s_i\}}$ is determined from the Hamiltonian (eq. 1). The partition function Z is: [1, 2, 6, 8]

$$Z = \sum_{\{s_i\}} e^{-\beta E_{\{s_i\}}}. \quad (11)$$

Step 2 in the algorithm is repeated until the system converges to the steady state of Markov chain thermal fluctuations [1]. In this converged state, the variance in $\frac{M}{M_s}$ due to these thermal fluctuations can be used to calculate χ_{eff} through eq. 3.

II.2 Thermalisation methods for ferromagnetism

To ensure the system has reached a thermalised state, where measurements of its properties are taken, various methods are considered for different circumstances. These methods have been categorised as follows:

1. Extrapolating from the convergence behaviour of the system.
2. Determine at what t the system has thermalised to then take data from there.
3. Having the number of thermal sweeps t so high that we expect it to be highly likely the system has been thermalised for a set interval at the end that data can be taken from.

These methods are investigated to minimise computing time necessary to obtain useful data.

II.2.1 Convergence fit

For J_{eff} or $\vec{\mathbf{B}}\mu$ getting larger with respect to the thermal energy $k_B T$, i.e. exchange & EM interactions becoming stronger than the thermal fluctuations before thermalisation, it becomes more likely for the system to thermalise with a direct path to its steady-state average. This can be seen in fig. 2. In this case, we can employ the first method outlined above as the convergence of $\frac{M}{M_s}$ can be fitted to an exponential curve:

$$\frac{M}{M_s} = e^{-(a \times t + b)} + \left(\frac{M}{M_s}\right)_{conv.}, \quad (12)$$

where t is the sweep number and a, b and $\left(\frac{M}{M_s}\right)_{conv.}$, the convergent value, are the fitting parameters. Fitting a curve

to the data gives an approximation for a final convergent value without guessing the t value at which the system has converged, $t_{conv.}$. This fit is performed using the chi-squared method on residuals, rather than the normalised residuals. The chi-squared method, throughout this work, has been performed using the Scipy.Optimize,Minimize function. As $\frac{J_{eff}}{k_B T}$ and $\frac{\vec{\mathbf{B}}\mu}{k_B T}$ get smaller, the thermalisation process becomes less consistent, which resulted in no fitting model having been utilised.

II.2.2 Adaptive thermalisation

The other two categories of thermalisation methods are based on taking the average, $\left\langle \frac{M}{M_s} \right\rangle$, on an interval of set length. The first of these two is the adaptive thermalisation, which determines the value of $t_{conv.}$ and consists of the following steps:

1. Initialise the system and perform an initial n number of sweeps.
2. Evaluate the convergence condition over the last n_{avg} number of sweeps.
3. If the condition is not met, perform another n_{avg} sweeps and go back to step 2.

Two conditions have been investigated:

- Comparing averages: The difference in average over the last n_{avg} and the last $2 \times n_{avg}$ sweeps must be smaller than a reference value.
- Standard deviation: The standard deviation, σ on the last n_{avg} must be smaller than a reference value, σ_{ref}.

The reference values have been determined empirically from thermalised systems, where the thermalisation has been discerned visually.

II.2.3 General thermalisation

The general method has n simply increased massively with the data then taken from the last n_{avg} points.

An additional tool, which reduces the impact of data from an unthermalised system on the results, is performing a weighted averaging over multiple simulations with the same parameters. This method also provides a way to incorporate this thermalisation uncertainty in the errors and obtain an average over the thermalised data, reducing random errors. If the data is taken to be normally distributed around the mean, $\approx 68.3\%$ of the data falls within $\pm\sigma$. Hence, when doing at least 3 simulations, the majority of the data is expected to fall within this interval, so that results within $\pm\sigma$ of the true mean will dominate over those lying further away. To balance this with the additional computing time, exactly 3 simulations have been done per data point.

II.3 Thermalisation methods for para- & antiferroamagnetism

In the paramagnetic phase, the spins are randomly aligned for $B = 0T$ when there is no hysteresis [4]. So, when the system is initialised randomly, it is already close to being thermalised, though not fully as the configuration of spins would follow a Gaussian rather than a Boltzmann distribution. Hence, to determine $\left\langle \frac{M}{M_s} \right\rangle$, using the general method n can be much lower than in the ferromagnetic phase.

For the antiferromagnetic phase, the spins are not randomly aligned but the system does not need to overcome opposing magnetisation domains that form during this process as is the case for the ferromagnetic phase [5]. These domains in the Ising model are called Peierls droplets [2] and are proportional to ζ. The method of adaptive thermalisation using the standard deviation as well as the general thermalisation method can be used. However, for the general method, n can be decreased compared to the ferromagnetic phase.

III Results

III.1 Thermalisation results

III.1.1 Convergence fit results

It was found that the model described in section II.2.1 can give an overestimate of the steady-state average. This can be seen from the distribution of points in the steady state in fig. 2, which gives a ratio of points above to points below the converged value of $\frac{0.14}{0.86}$. This regards all points with $t > 50$. On the other hand, simply taking the average of all $\frac{M}{M_s}$ with $t > 50$, gives us a value for this ratio of $\frac{0.64}{0.36}$, which is closer to the ratio around the thermal average in the Boltzmann distribution of $\approx \frac{0.63}{0.37}$. Additionally, when comparing these two methods using their reduced chi-squared value on this interval, χ^2_ν [12], it is found to be $\approx 1.92\times$ higher than for the simple average. As these relative results are consistently obtained from different simulations and these direct thermalisation paths do not occur often enough for the values of $\frac{J_{eff}}{k_B T}$ that are investigated, the method of averaging from a given t has been chosen over the exponential fit method.

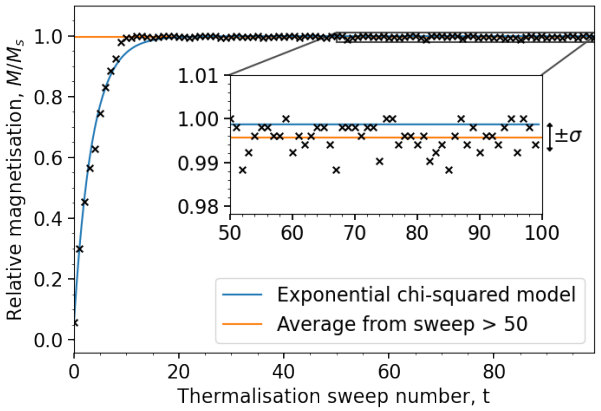

Figure 2: The relative magnetisation over 100 thermalisation sweeps of a 32×32 lattice with $\frac{\mu B}{k_B T} = 0.02$ and $\frac{J_{eff}}{k_B T} = 0.8$. The two methods to obtain the steady-state average are plotted: an exponential Chi-squared fit and an average from sweep > 50. The $\pm$ standard deviation interval is marked based on the latter method.

III.1.2 Adaptive thermalisation results

Whilst converging, it is found that the system can show oscillatory behaviour as well as temporary unstable equilibrium states. Taking n_{avg} to be large enough to negate the effect of these unstable equilibria on the convergence test, instead causes the average to be taken over the full oscillatory behaviour. This means that $\left\langle \frac{M}{M_s} \right\rangle$ can be the same for consecutive n_{avg} without the system having converged. On the other hand, σ on $\frac{M}{M_s}$ does take this

oscillatory behaviour into account, which means it can provide a more reliable test of convergence. However, as σ has been found to increase rapidly as T gets close to T_c, this method cannot be used as well in that range because σ_{ref} would need to be adjusted for many small intervals and the difference in σ between convergence & non-convergence gets smaller. This behaviour in σ can be seen in figures 3 & 4, where χ_{eff} increases substantially as T goes to T_c and then so does σ, using eq. 3.

Therefore, when taking measurements for $\left\langle \frac{M}{M_s} \right\rangle$ and χ_{eff} over T, the data has been split up in three intervals: one for T around T_c and then one for larger and one for smaller T. The latter makes use of the adaptive thermalisation, whilst the other two use the general thermalisation method. It was found that a safe σ_{ref} for thermalisation is ≈ 0.178. When T is close to T_c the thermal fluctuations were found to be strong enough so that the system can leave its thermalised state, thus making the weighted fit over multiple simulations even more important in this region to improve the data.

III.2 Ferromagnetic phase transition

$\left\langle \frac{M}{M_s} \right\rangle$ and χ_{eff} have been plotted against $\frac{k_B T}{J_{eff}}$ for 6 lattice sizes in fig. 3. The normalised residuals, R indicate that

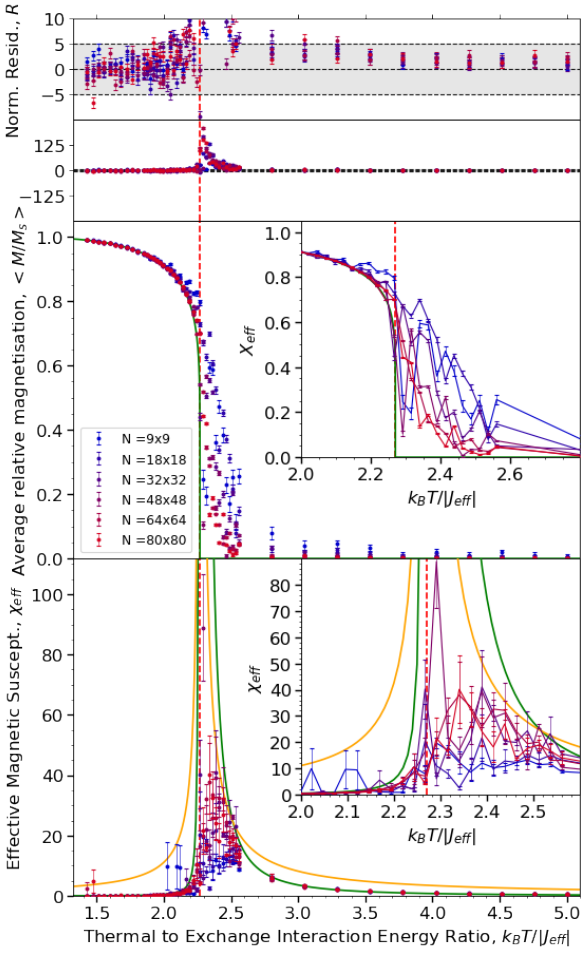

Figure 3: The average relative magnetisation and zero-field effective magnetic susceptibility over $\frac{k_B T}{J_{eff}}$ for different lattice sizes. The red dashed line marks $\frac{k_B T_c}{J_{eff}}$, the Onsager model magnetisation and susceptibility is plotted in green and the Curie-Weiss model in yellow. Normalised residuals on the magnetisation are plotted twice at the top.

the data follow the Onsager solution 4 well in the ferro- and paramagnetic phase though diverge from it around the phase transition. The 1st derivative of the Onsager solution with respect to $\frac{k_B T}{J_{eff}}$ diverges to $-\infty$ with a discontinuous change to 0 at $T = T_c$, though this change in the derivative is smoothed out for the computational results. However, the width of this smoothing can be seen to decrease for larger N as the data gets closer to the onsager solution. However, whilst the residuals do, the values for R not appear to decrease for larger N. χ_{eff} increases towards T_c from both sides and is smaller with a sharper increase as T goes to T_c from the left, as expected from eq. 5 & 7. Generally, this increase in χ_{eff} becomes larger for larger N, thus getting closer to a $(T - T_c)^{-\gamma}$ curve for $\gamma > 0$. Two sets of curves have been fitted visually representing the general form of the Curie-Weiss and Onsager models, using their critical exponents and the ratio between proportionality constants (Curie constants) C on either side of the interval. Comparing the two in the paramagnetic phase, the data follows $\gamma = 7/4$ much better than $\gamma = 1$. Furthermore, particularly due to the proportionality constant of the Landau model, the Curie-Weiss curve describes the data less well than the Onsager model.

III.2.1 Chi-squared fit

Closest to the thermodynamic limit, the $N = 80 \times 80$ model has been isolated in fig. 4. From fig. 3, the data diverges from the theoretical curves around T_c, hence an interval of data points around T_c has been excluded for fitting in order to obtain a model that matches the thermodynamic limit most. One model uses $\gamma = 7/4$ whilst the other determines γ through the fit. The obtained model and statistical parameters are stated in table 1. The ratio of R within ± 5 makes the general fit a better fit though, the percentages are still much lower than the normal distribution 99.99994%. Additionally, the Durbin-Watson statistic $\mathcal{D}$ indicates that the residuals are somewhat systematically correlated, as $\mathcal{D} = 0$ represents systematically correlated and $\mathcal{D} = 2$ normal distributed residuals [12]. Moreover, the $\chi^2_\nu >> 1$ indicates the fits definitely ought to be questioned. All these parameters indicate that the general fit is much better than the Onsager fit, though still does not provide a satisfactory model. Note however, that $\mathcal{D}$ actually states that the Onsager fit provides less correlated residuals than the general fit for $T < T_c$.

Model:	Onsager $T < T_c$	Onsager $T > T_c$	General $T < T_c$	General $T > T_c$
Curie constant, $C\ (K^{-1})$	$0.00845 \pm 6e-5$	$2.347 \pm 6e-3$	$0.756 \pm 3e-3$	$2.347 \pm 6e-4$
Critical exponent, γ	$7/4$	$7/4$	$2.009246 \pm 9e-6$	$1.380 \pm 5e-4$
$\mathcal{D}$	0.68	1.00	1.05	0.89
$\lvert R \rvert \leq 5$	25.9%	52.9%	77.8%	88.6%
χ^2_ν	364.6	276.1	189.1	11.01

Table 1: The parameters of the ferromagnetic Curie-Weiss and Onsager fit with their fitting parameters: the Durbin-Watson statistic $\mathcal{D}$, the ratio of normalised residuals within ± 5 and the reduced chi-squared value χ^2_ν.

III.3 Antiferromagnetic phase transition

χ_{eff} for 14 lattice sizes as well as the difference in χ_{eff} between different lattice sizes has been plotted against $\frac{k_B T}{J_{eff}}$ in fig. 5. The peak in χ_{eff} which is at T_N does not lie at the T_c calculated from the Onsager solution, which agreed

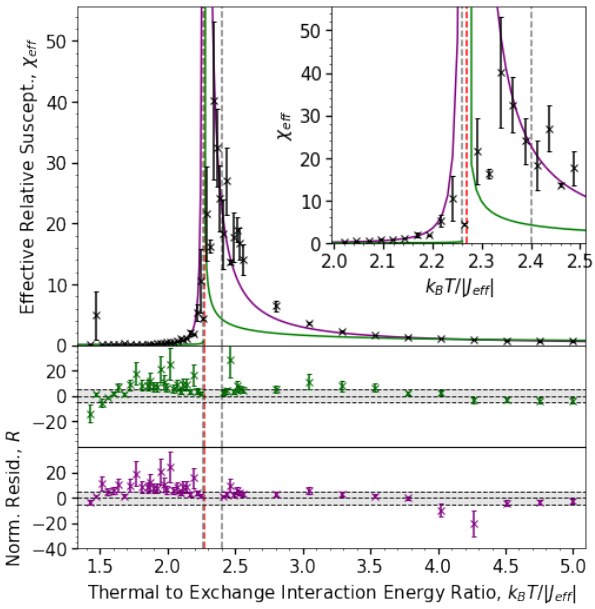

Figure 4: The zero-field χ_{eff} over $\frac{k_BT}{J_{eff}}$ for a 80×80 lattice. The red dashed line marks $\frac{k_BT_c}{J_{eff}}$, the onsager solution is plotted in green and a general solution in purple. Their normalised residuals are plotted the bottom in their respective colours. The interval of the data excluded from fitting is marked by grey dashed lines.

well with the computational results for the ferromagnet, thus disagreeing with Weiss' theory. The data does however show a smooth curve up to T_N as predicted by Néel's theory. Comparing the different lattice sizes, unlike in the ferromagnetic case, no clear pattern has been observed, with the system showing similar behaviour irrespective of size.

III.3.1 Chi-squared fit

The $N = 32 \times 32$ has been isolated and plotted in fig. 6 as the most data has been generated for it, also with the largest t. From fig. 5, the results from this system should thus provide the most accurate representation of a antiferromagnetic system as described in section I.1. As T_N is thus not given by the Onsager model, an iterative method has been used to calculate it. From an initial estimate of T_N, models are fitted using the chi-squared method against the data in the $T < T_N$ and $T >= T_N$ regime respectively. T_N is then reevaluated as the point of intersect between the two obtained curves. This process is repeated 10 times.

However, as shown in fig. 6, the model described in eq. 9 provides a bad fit with $\chi^2_\nu = 279.7$, as can be seen in fig. 6. Instead, a phenomenological model has been used:

$$\chi_0 = a_0 \times \left(\frac{k_BT}{J_{eff}}\right) + a_1 \times \left(\frac{k_BT}{J_{eff}}\right)^2 + a_3 \times \left(\frac{k_BT}{J_{eff}}\right)^3, \tag{13}$$

a 3rd order polynomial which has $\chi_{eff} = 0$ at $T = 0\ K$ as required by Néel's theory.

The obtained parameters are found in table 2 and the statistical fitting parameters are found in table 3. $\mathcal{D}$ indicates that the normalised residuals, R, for the Weiss model are somewhat correlated. When comparing this to the R as well as the χ_{eff} data in the graph, it seems the data follows a flatter line rather than the curve plotted there, i.e. a lower critical exponent than $\gamma = 1$. This is also supported by the distribution plot, which is slightly offset to the left, showing more values above the curve, though with a few

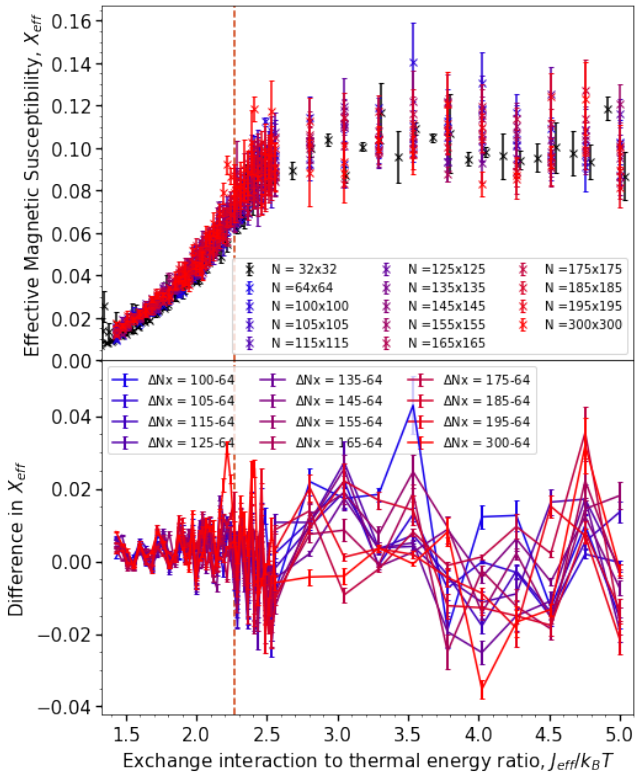

Figure 5: The zero-field χ_{eff} and the difference in χ_{eff}, with respect to a 64×64 lattice, over $\frac{k_BT}{J_{eff}}$ for different lattice sizes. The orange dashed line marks $\frac{k_BT_c}{J_{eff}}$.

much further lying points below. Looking at where these residuals above and below 0 lie, having a flatter line would shift this distribution closer to the centre. The number of norm. residuals within ± 3 is much lower than the normal distribution 99.7%. Both values for χ^2_ν indicate the fits should be questioned, though it does support the phenomenological model over the quadratic model.

$\frac{k_BT_N}{J_{eff}}$	$C, (K^{-1})$	a_0	a_1	a_2
≈ 2.556	$(7.21 \pm 0.04)e-1$	$(2.31 \pm 0.10)e-3$	$(-1.017 \pm 0.016)e-2$	$(9.48 \pm 0.07)e-3$

Table 2: The model parameters of the antiferromagnetic Weiss and phenomenological fit.

Model:	$\mathcal{D}$	$\lvert R\rvert \leq 3$	χ^2_ν
Weiss	1.33	72.9%	21.79
Phenomenological	1.60	86.1%	5.75

Table 3: The statistical fitting parameters of the antiferromagnetic Weiss and phenomenological fit.

IV Discussion

Comparing the two fits for the ferromagnetic system, the different critical exponents (table 1) above and below T_c and different from the Onsager solution thus provide a better fit. However, the reduced Chi-squared values for either fit would still question them. Similarly for the antiferromagnet, the data supports slightly different critical exponents, that being a 3rd order polynomial rather than a quadratic function below T_N and a lower critical exponent above it. Though better, the reduced Chi-squared values indicate that the fits should be questioned. However, these high values may be because of errors which are too small and instead the relative differences are more important. The errors do not take the difference in system sizes into account, which makes them an underestimate when we fit the data to general curves with critical exponents derived in the thermodynamic limit. In

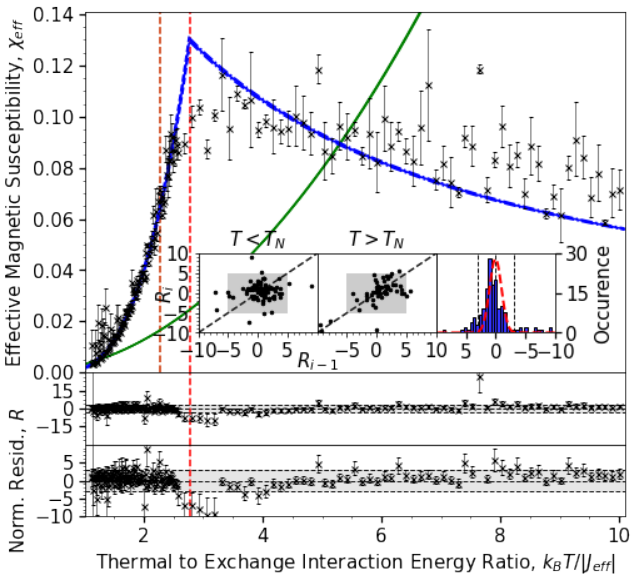

Figure 6: The zero-field χ_{eff} over $\frac{k_BT}{J_{eff}}$ for a 32×32 lattice. The red and orange dashed lines mark the obtained $\frac{k_BT_N}{J_{eff}}$ & Onsager $\frac{k_BT_c}{J_{eff}}$ and the phenomenological & Weiss model are plotted in blue. Their normalised residuals are plotted twice on the bottom with their distribution as well as the lag plots for each regime shown in the centre. The quadratic model is plotted in green. The errors on the model parameters are shown as a interval around their curves.

the ferro- and paramagnetic phase of the ferromagnet, these errors skew the onsager fits to become very flat, which makes them disagree with the points close to the phase transition. Fits using points solely around the phase transition have been investigated, though whilst the errors are not too small here, the data is not close to the thermodynamic limit. This is because of the correlation length diverging at T_c, which causes it to be larger than the size of the lattice. This explains why generally the smaller systems reach there max value of χ_{eff} quicker, as it reaches the limits due to its size for more values of T. Additionally, a value for n_{avg} of 200 has generally been used which was seen to work well. However, a better value could have been approximated by comparing it to the Boltzmann distribution to see how large n_{avg} should be for it to represent the distribution well.

V Conclusions

The computational data obtained follows the general trend of the solution of the Ising model obtained by Onsager much better than Curie-Weiss' mean-field theory, though exact fits of the magnetic susceptibility indicate that the critical exponents should be higher for the paramagnetic phase and lower for the ferromagnetic phase. The quadratic model describing the magnetic susceptibility in the antiferromagnetic phase does not agree well with the data and instead a phenomenological model has been determined to fit to it. Weiss' model fot the susceptibility in the paramagnetic phase generally agrees well though the data indicates a lower critical exponent.

References

[1] Landau, R. H., Jose, M.,& Bordeianu, C. C. (2015). Computational physics : problem solving with Python. Wiley-Vch. C.

[2] Tong, D. (2012, May). David Tong: Statistical Physics. www.damtp.cam.ac.uk; University of Cambridge. https://www.damtp.cam.ac.uk/user/tong/statphys.html

[3] Wang, H. et al. (2010). Exchange interaction function for spin-lattice coupling in bcc iron. Physical Review B, 82(14). https://doi.org/10.1103/physrevb.82.144304

[4] Mccoy, B. M., & Wu, T. T. (1973). The two-dimensional Ising Model. Harvard University Press.

[5] Kittel, C. (2005). Introduction to solid state physics (8th ed.). John Wiley & Sons, Inc.

[6] Pathria, R. K., & Beale, P. D. (2011). Statistical Mechanics. (3rd ed.). Elsevier Academic Press.

[7] Landau, D. P., & Binder, K. (2005). A Guide to Monte Carlo Simulations in Statistical Physics. Cambridge University Press.

[8] Cai, W. (2011). ME346A Introduction to Statistical Mechanics (Handout 12. Ising Model). Stanford University.

[9] Onsager, L. (1944). Crystal Statistics. I. A Two-Dimensional Model with an Order-Disorder Transition. Physical Review, 65(3-4), 117–149. https://doi.org/10.1103/physrev.65.117

[10] Tessman, J. R. (1952). The Parallel Susceptibility of an Antiferromagnet at Low Temperatures. Physical Review, 88(5), 1132–1137. https://doi.org/10.1103/physrev.88.1132

[11] Metropolis, N., Rosenbluth, A. W., Rosenbluth, M. N., Teller, A. H., Teller, E. (1953). Equation of State Calculations by Fast Computing Machines. The Journal of Chemical Physics, 21(6), 1087–1092. https://doi.org/10.1063/1.1699114

[12] I. G. Hughes, T. P. A. Hase, Measurements and their Uncertainties, A practical guide to modern error analysis, Oxford university press, New York, United States (2010).